

## Article

# Degradation of Tetracycline in Water by Fe-Modified *Sterculia Foetida* Biochar Activated Peroxodisulfate

Yuchen Zhang<sup>1</sup>, Xigai Jia<sup>1</sup>, Ziyang Kang<sup>1</sup>, Xiaoxuan Kang<sup>1</sup>, Ming Ge<sup>1</sup>, Dongbin Zhang<sup>2</sup>, Jilun Wei<sup>2</sup>, Chongqing Wang<sup>3,\*</sup>  and Zhangxing He<sup>1,4,\*</sup>

<sup>1</sup> College of Chemical Engineering, North China University of Science and Technology, Tangshan 063210, China

<sup>2</sup> Tangshan Sanyou Group Xingda Chemical Fiber Co., Ltd., Tangshan 063305, China

<sup>3</sup> School of Chemical Engineering, Zhengzhou University, Zhengzhou 450001, China

<sup>4</sup> Tangshan Sanyou Group Co., Ltd., Tangshan 063305, China

\* Correspondence: cqwang1990@zzu.edu.cn (C.W.); zxhe@ncst.edu.cn (Z.H.)

**Abstract:** Tetracycline (TC) is a broad-spectrum antibiotic commonly, made use of in aquaculture and animal husbandry. After entering water bodies, it will represent a major threat to human health. In this study, *sterculia foetida* biochar (SFC) was readied by the combined hydrothermal pyrolysis (co-HTP) method with *sterculia foetida* as raw materials. Fe-SFC (Fe<sub>2</sub>-SFC, Fe<sub>3</sub>-SFC, and Fe<sub>4</sub>-SFC) was obtained by doping SFH with different concentrations of FeCl<sub>3</sub>. Finally, activation of peroxodisulfate (PDS) was achieved, using Fe<sub>3</sub>-SFC to degrade TC. The degradation of TC obeyed pseudo-second-order kinetics, and the constant of the reaction rate was 0.491 L mg<sup>-1</sup> min<sup>-1</sup>. Radical trapping experiments, EPR test and electrochemical tests evidenced that the high catalytic performance of the Fe<sub>3</sub>-SFC/PDS system was ascribed to free radical pathway (•OH and SO<sub>4</sub>•<sup>-</sup>) and non-radical pathway (<sup>1</sup>O<sub>2</sub> and electron transfer), in which the latter plays a dominant role. This research not only demonstrates a new kind of biochar as an effective catalyst for PS activation, but also offers an avenue for the value-added reuse of *sterculia foetida*.



check for updates

**Citation:** Zhang, Y.; Jia, X.; Kang, Z.; Kang, X.; Ge, M.; Zhang, D.; Wei, J.; Wang, C.; He, Z. Degradation of Tetracycline in Water by Fe-Modified *Sterculia Foetida* Biochar Activated Peroxodisulfate. *Sustainability* **2022**, *14*, 12097. <https://doi.org/10.3390/su141912097>

Academic Editor: Francesco Granata

Received: 21 August 2022

Accepted: 20 September 2022

Published: 24 September 2022

**Publisher's Note:** MDPI stays neutral with regard to jurisdictional claims in published maps and institutional affiliations.



**Copyright:** © 2022 by the authors. Licensee MDPI, Basel, Switzerland. This article is an open access article distributed under the terms and conditions of the Creative Commons Attribution (CC BY) license (<https://creativecommons.org/licenses/by/4.0/>).

**Keywords:** peroxydisulfate activation; biochar; *sterculia foetida*; tetracycline wastewater; degradation

## 1. Introduction

Tetracycline (TC) as a broad-spectrum antibiotic has been diffusely made use of in clinical medicine and animal husbandry, and TC is usually discharged into the environment through medical wastewater and domestic wastewater [1–3]. Due to the poor biodegradability of TC, it may accumulate in the environment for a long time [4]. Many studies have indicated that after entering the aquatic environment [5], TC can cause the production of antibiotic resistance genes, boost bacterial resistance and cause ecotoxicity [6,7]. This will endanger human health and ecosystem stability [8]. As a result, an effective technique to degradation of TC in the water bodies is required [9,10].

Advanced oxidation processes (AOP) have shown great efficiency and almost non-selectivity in treating pollutants, when compared to traditional approaches [11,12]. A valid method for degrading organic contaminants in wastewater is the persulfate (PS)-based advanced oxidation process (AOP) [13,14]. Peroxymonosulfate (PMS) and peroxodisulfate (PDS) are two PS oxidants [15]. However, PS alone has a low degradation efficiency for antibiotics [16]. Various methods [17], such as photocatalytic [18], heating [19], UV light [20] and transition metals [19], can generate reactive oxygen species (ROS) by activating PS, but these methods suffer from energy requirements, metal leaching, and other disadvantages. Research shows PS can be activated by carbon-based materials [21] such as carbon nanotubes (CNT) [22], activated carbon (AC) [23], biochar (BC) [24], and reduced graphene oxide (r-GO) [25], etc. Due to the advantages of abundant raw materials, low cost [26], rich mesoporous structure [27], and surface functional groups [28], BC produced from biochar waste has increasingly become a current research hotspot [23,29,30].

Modified BC doped with transition metals and heteroatoms is often utilized to prepare catalysts to improve the catalytic activity of BC [10,31,32]. Given Fe-based catalysts' high PS activation efficiency, combining biochar with iron-based materials to improve PS activation efficiency has received extensive attention [29]. As an activator, ferric chloride ( $\text{FeCl}_3$ ) [33] can enhance the accessible surface area of carbon materials while maintaining good electrical conductivity [34], promoting the adsorption of pollutants and electron transfer. Luo [29] et al. developed iron-rich magnetic BC (KMBC)-activated PS to efficiently degrade metronidazole, with a degradation rate of 98.4% after 120 min, and discovered that active ingredient content in magnetic BC [35], particularly the content of Fe, (II) was closely related to its activation properties [36,37].

BC was made in this work using *sterculia foetida* as a raw material [38,39]. The *sterculia foetida* was first subjected to hydrothermal treatment and then calcined to obtain SFC. Using  $\text{FeCl}_3$  as the precursor, iron-modified BC with different ratios ( $\text{Fe}_2$ -SFC,  $\text{Fe}_3$ -SFC, and  $\text{Fe}_4$ -SFC) were further prepared. The degradation performance of the produced materials and SFC were compared when they were utilized to degrade TC. The catalysts' characteristics were examined by approaches for characterization [40] such as scanning electron microscopy (SEM), transmission electron microscopy (TEM), X-ray diffraction (XRD), Raman spectroscopy, BET surface area measurements, and X-ray photoelectron spectroscopy (XPS). The influences of certain factors (catalyst dosage, oxidizer dosage, solution temperatures, solution pH, concentration of initial, coexisting anions, etc.) on the removal of TC in  $\text{Fe}_3$ -SFC/PDS system were probed. Finally, the mechanism of  $\text{Fe}_3$ -SFC-activated PDS for TC degradation was brought forwards [41].

In this study, the Fe element is doped with *sterculia foetida* biochar to prepare iron-based biochar catalysts for the first time, which keeps carbon materials' high electrical conductivity and larger accessible surface area, and provides a more novel and efficient method for the value-added utilization of *sterculia foetida*. At the same time, the above materials are used as catalysts, and peroxydisulfate activation is used to achieve more efficient TC degradation under non-selective conditions and broaden the removal path of water pollutants.

## 2. Materials and Methods

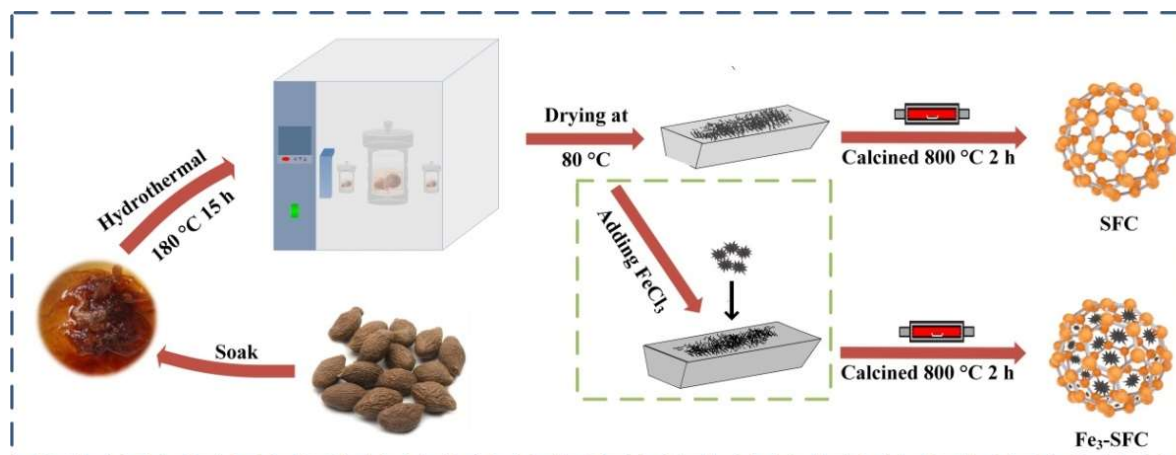
### 2.1. Materials

*Sterculia foetida* was purchased from the supermarket. Absolute ethanol (purity > 99.7%), sodium hydroxide ( $\text{NaOH}$ , analytical reagent), sulphury acid ( $\text{H}_2\text{SO}_4$ , analytical reagent), sodium bicarbonate ( $\text{NaHCO}_3$ , analytical reagent), and sodium phosphate ( $\text{Na}_3\text{PO}_4$ , analytical reagent) were obtained from Tianjin Yong Da Chemical Reagent Co., Ltd. Tetracycline (TC, analytical reagent) was purchased from Aladdin Industrial Corporation. Ethanol ( $\text{EtOH}$ , chromatographic grade) was acquired from China Shanghai Aladdin Biochemical Technology Co., Ltd. Anhydrous ferric chloride ( $\text{FeCl}_3$ , analytical reagent) and Sodium persulfate ( $\text{Na}_2\text{S}_2\text{O}_8$ , analytical reagent) were obtained from Shanghai Macklin Biochemical Co., Ltd. (Shanghai, China) Sodium nitrate Tianjin Bai Shi Chemical Industry Co., Ltd. (Tianjin, China) provided the analytical reagents Tertbutyl alcohol (TBA,  $\text{C}_4\text{H}_{10}\text{O}$ ), sodium chloride ( $\text{NaCl}$ , analytical reagent), and sodium nitrate ( $\text{NaNO}_3$ , analytical reagent). Alfa Esha (China) Chemical Co., Ltd. (Shanghai, China) supplied the furfuryl alcohol (FFA,  $\text{C}_5\text{H}_6\text{O}_2$ , purity > 98%).

### 2.2. Biochar-Based Catalyst Synthesis

*Sterculia foetidus* was soaked for 2 h in 1000 mL distilled water. The fruit cores were removed and filtered after the *sterculia foetidus* were soaked to expand, then diverted to five 100 mL autoclaves and heated for 18 h at  $180\text{ }^\circ\text{C}$ , and then cooled to room temperature. After washing and filtering the product with distilled water and hydrous ethanol, hydrothermal biochar (SFH) was obtained. It was placed inside a tubular reactor and calcined for 2 h at  $800\text{ }^\circ\text{C}$  in a  $\text{N}_2$  environment to produce blank calcined biochar (SFC). After mixing and grinding the mass of SFH and  $\text{FeCl}_3$  in a certain ratio (1:2; 1:3 and 1:4), it was placed in

a tubular reactor to calcine the obtained material under the same conditions, and then soaked in 0.1 mM HCl solution for 12 h, according to the ratio of 0.5 g material to 200 mL hydrochloric acid solution. After filtration, the product was centrifuged and washed with distilled water to get Fe-doped FeCl<sub>3</sub>-modified biochar (Fe<sub>2</sub>-SFC; Fe<sub>3</sub>-SFC and Fe<sub>4</sub>-SFC). The material preparation method is shown in Scheme 1.



**Scheme 1.** Schematic representation of the preparation of SFC and Fe<sub>n</sub>-SFC.

### 2.3. Characterization

Fourier transform infrared spectroscopy was used to identify the Fourier transform infrared (FT-IR, D-76275 Ettlingen Germany) of SFC and Fe<sub>3</sub>-SFC as KBr (mass ratio of 1:400) pellets, before and after use. The D8-X-ray diffractometer (Bruker Company, Bremen, Germany) was used to find the obtained sample's XRD diffraction pattern. To examine the catalyst's morphology, a scanning electron microscope (SEM, JEOL, JSM-6390LV) was employed. The BET surface area, pore size, and pore volume of the catalyst were determined using a specific surface area pore size analyzer (Beijing Beishi Shi De Instrument Technology Co., Ltd., 3H2000PM1 Beijing China). X-ray photoelectron spectroscopy (Thermo KAlpha XPS America) was used to determine elemental valence of the catalyst. An electron spin resonance spectrometer (EPR) was used to detect the free radicals produced in the BC/PDS system.

### 2.4. Catalytic Degradation Experiment

In a typical method, 10 mg of biochar catalyst and 100 mL of 20 mg/L TC solution were added into a 250 mL beaker, and ultrasonic treatment was carried out for 1 min. It was quickly transferred to a water bath, stirred at 400 r/min, and 100 mg of PDS was added to the beaker solution to start the degradation reaction after 15 s of stirring. A certain amount of the sample solution (3 mL) was removed in a given time (0, 1, 2, 5, 10, 20, 40, 60 min), and filtered with 0.45 μm polyethersulfone membrane. The absorbance of the filtrate was immediately detected by UV-V spectrophotometer at λ = 359.5 nm.

Without special instructions, all experiments were performed under the conditions of temperature 25 °C, pH 6.93, and initial TC concentration of 20 mg/L, with no adjustment required. The effects of different kinds of biochar on TC degradation were studied by using the above method, and the first-order and second-order kinetics analyses were made. Different biochar concentrations (0.05 g/L, 0.10 g/L and 0.15 g/L), different PDS concentrations (0.5 g/L, 1.0 g/L and 1.5 g/L), different pH values (3.01, 6.93 and 11.03), different TC concentrations (10 mg/L, 20 mg/L and 30 mg/L), different temperatures (25 °C, 35 °C and 45 °C) and different anions (Cl<sup>-</sup>, NO<sub>3</sub><sup>-</sup>, HPO<sub>4</sub><sup>2-</sup>, HCO<sub>3</sub><sup>-</sup>) of the TC degradation were investigated. The free radical capture experiment and carbon cycle experiment in the process of TC degradation were tested.

### 2.5. Electrochemical Test

Preparation of the working electrode was as follows: 20 mg biochar was combined with 2 mL ethanol for 3 h of ultrasonic treatment, then dropped on the glassy carbon electrode, dried for 10 min at 60 °C, and then left to stand at 25 °C for 4 h. Platinum wire electrode was a counter-electrode, saturated calomel electrode was the reference electrode, with 50 mM Na<sub>2</sub>SO<sub>4</sub> as the electrolyte.

Linear sweep voltammetry (LSV), cyclic voltammetry (CV) and electrochemical impedance spectroscopy (EIS) were implemented at the electrochemical workstation (Chi660e, Shanghai CH Instrument Technology Co., Ltd.). The LSV diagram of SFC under different conditions (separate SFC, SFC + PDS and SFC + PDS + TC) was measured at 0.05 V/s sweep speed and −1.0–1.5 V potential. At the same time, the LSV of Fe<sub>3</sub>-SFC was measured at the same method and experimental conditions. At −1.5~1.5 V potential and 0.005 V/s scanning speed, the cyclic voltammetry (CV) curves of SFC and Fe<sub>3</sub>-SFC were measured. EIS was measured with an amplitude of 0.005 V and a range of 10<sup>−1</sup>~10<sup>5</sup> Hz in frequency.

## 3. Results and Discussion

### 3.1. Characterization

The changes in surface functional groups before and after the reaction of SFC and Fe<sub>3</sub>-SFC are shown in Figure 1a,b using FT-IR analysis. C-H (610 cm<sup>−1</sup>) [42], C-OH/C-O-C (1100 cm<sup>−1</sup>) [43], C-N (1380 cm<sup>−1</sup>) [44] and -OH/-NH<sub>2</sub> (1570, 3420 cm<sup>−1</sup>) [45] are the main tensile vibration functional groups of SFC, and these functional groups also react with Fe<sub>3</sub>-SFC. The stretching vibration frequency of C-OH/C-O-C in Fe<sub>3</sub>-SFC is higher than in SFC, whereas the stretching vibration of C-N, and -OH/-NH<sub>2</sub> is more noticeable in SFC. The bands in SFC are slightly different from Fe<sub>3</sub>-SFC in the FT-IR spectra [46], and the functional groups on the surface of the two materials changed before and after the reaction, indicating that these surface functional groups make an important impact in catalytic degradation [47,48]. The functional groups on its surface will react with PDS, and its main reaction equation is [3]:

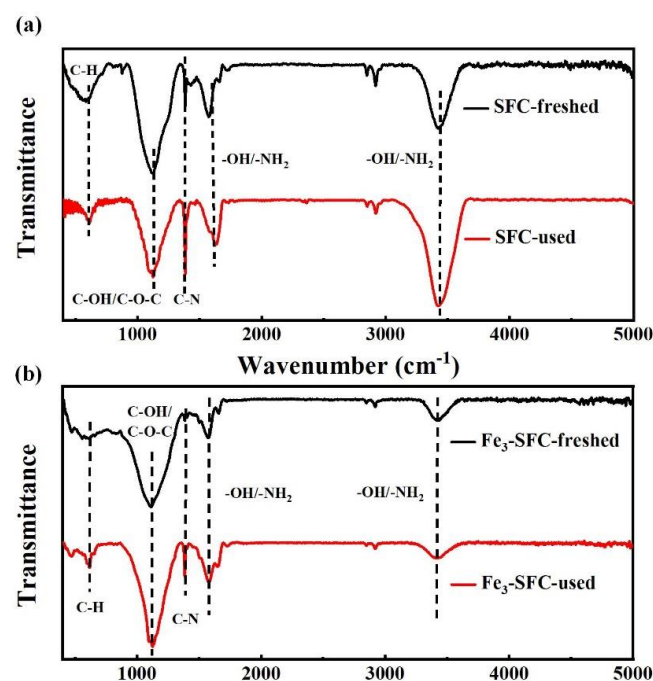
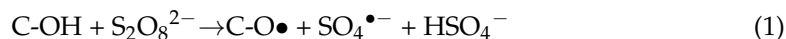
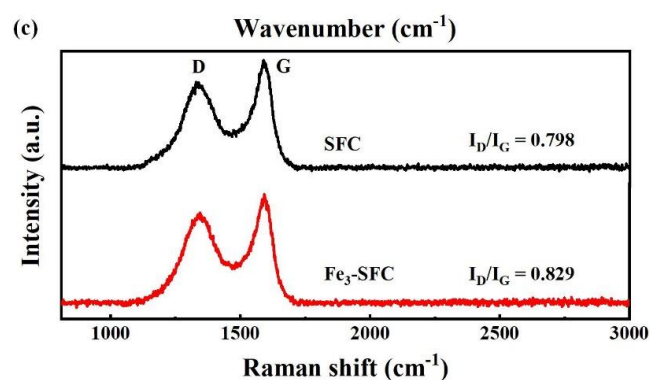


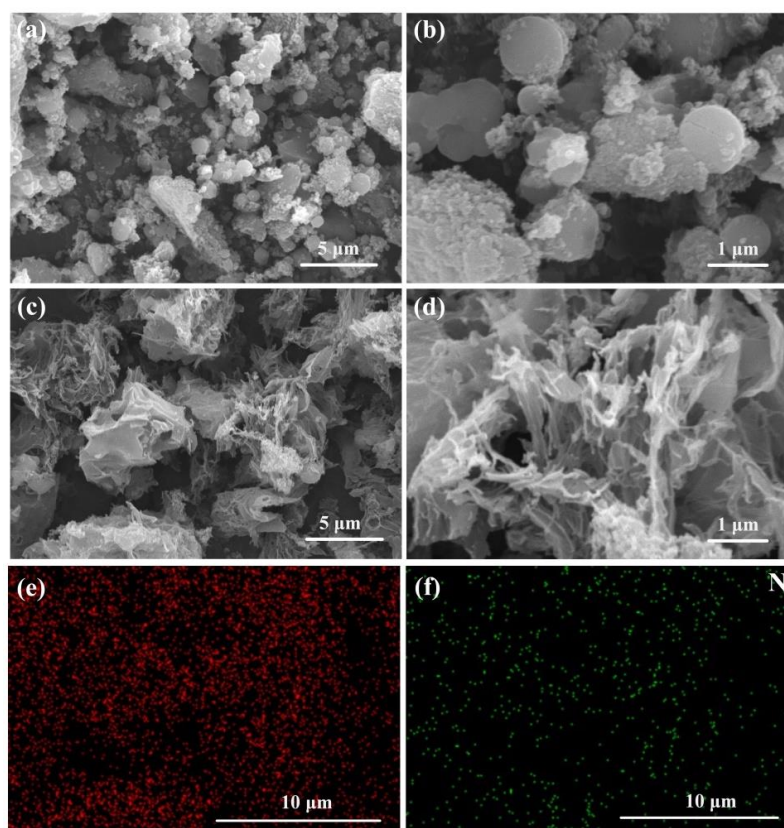
Figure 1. Cont.



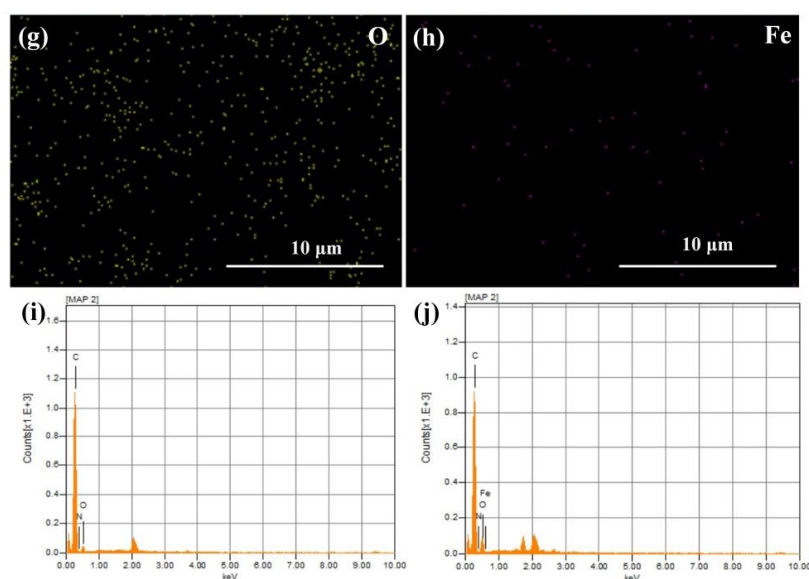
**Figure 1.** FT-IR spectra of the two materials before and after TC adsorption (a,b); Raman spectra of SFC and Fe<sub>3</sub>-SFC (c).

Figure 1c shows the Raman spectra of SFC and Fe<sub>3</sub>-SFC. The D and the G bands of the carbon material are represented by the peaks at 1350 and 1590 cm<sup>-1</sup> [49], respectively. SFC and Fe<sub>3</sub>-SFC have  $I_D/I_G$  values of 0.798 and 0.829, respectively, indicating that Fe<sub>3</sub>-SFC has more defects than SFC, which can supply more defect sites for PDS to activate the catalytic performance of biochar [50,51].

SEM images of SFC and Fe<sub>3</sub>-SFC are shown in Figure 2a–d. Although both SFC and Fe<sub>3</sub>-SFC are composed of granular structures, there are significant differences in material morphology between the two catalysts [52]. Fe<sub>3</sub>-SFC has larger particles and irregular surface roughness due to the incorporation of a small amount of Fe, while SFC exhibits relatively regular small particle shapes with smooth and more regular surfaces. As shown in Figure 2e–h, Fe<sub>3</sub>-SFC contains C, N, O and Fe elements, the distribution is relatively uniform, and the content of Fe element is relatively low. Figure 2i,g again shows that both SFC and Fe<sub>3</sub>-SFC contain the elements C, N and O, and that Fe<sub>3</sub>-SFC also contains the Fe element.



**Figure 2.** Cont.



**Figure 2.** SEM images of SFC (a,b) and Fe<sub>3</sub>-SFC (c,d); EDS mapping of Fe<sub>3</sub>-SFC (e-h); EDS spectra of SFC (i); EDS spectra of Fe<sub>3</sub>-SFC (j).

The crystal structure of the obtained carbon catalyst was investigated using XRD measurements. As shown in Figure 3, the diffraction peaks of SFC, Fe<sub>3</sub>-SFC and Fe<sub>3</sub>-SFC used at  $2\theta$  are at  $20.8^\circ$ , which corresponds to the (002) graphite structural plane [53]. At the same time, no other peaks were added after the modification of Fe, which indicated that most of Fe did not remain on the surface or inside of biochar, and Fe changed the structure of biochar during calcination. The peaks of Fe<sub>3</sub>-SFC did not change significantly after use, which proves that Fe<sub>3</sub>-SFC has good stability.

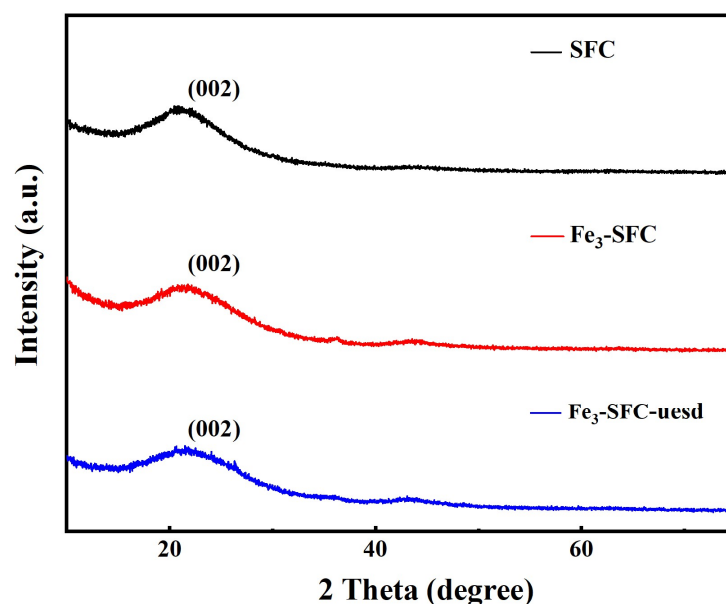


**Figure 3.** XRD patterns of SFC; Fe<sub>3</sub>-SFC and Fe<sub>3</sub>-SFC after use.

The N<sub>2</sub> adsorption and desorption isotherms of SFC and Fe<sub>3</sub>-SFC are demonstrated in Figure 4a. SFC and Fe<sub>3</sub>-SFC are shown as typical type II isotherms [54]. Fe<sub>3</sub>-SFC can offer more active sites for the activation of PDS, since both its BET surface area and pore volume are greater than those of SFC (Table 1) at  $959.2110 \text{ m}^2/\text{g}$  and  $1.0152 \text{ cm}^3/\text{g}$ , respectively (Table 1) [52,55]. Figure 4b shows the pore size–distribution curves of SFC and Fe<sub>3</sub>-SFC. Transition pores and micropores are found in both SFC and Fe<sub>3</sub>-SFC [56].

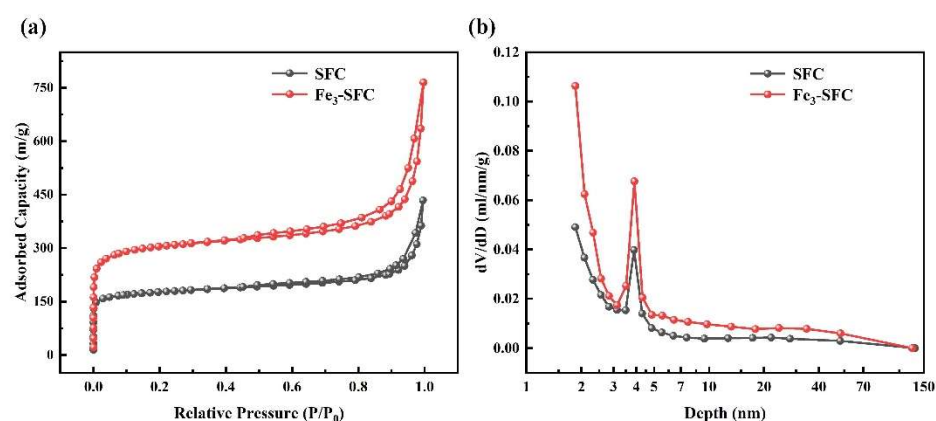


**Figure 4.** N<sub>2</sub> adsorption–desorption isotherms (a); and pore–size distribution curve (b).

**Table 1.** Specific surface area and pore volume of SFC and Fe<sub>3</sub>-SFC.

Sample	Surface Area (m <sup>2</sup> /g)	Pore Volume (cm <sup>3</sup> /g)
SFC	558.5050	0.5649
Fe <sub>3</sub> -SFC	959.2110	1.0152

The chemical composition and morphology of SFC and Fe<sub>3</sub>-SFC were analyzed using XPS, shown in Figure 5. According to XPS results, both SFC and Fe<sub>3</sub>-SFC contain C, N, and O elements, and Fe<sub>3</sub>-SFC also contains Fe (Figure 5a). The atomic content ratios of C, N, O and Fe in SFC and Fe<sub>3</sub>-SFC are shown in Figure 5b. It shows that the C content of Fe<sub>3</sub>-SFC after Fe doping is relatively lower than that of SFC. Meanwhile, the content of N and O increases, which provides more functional groups, and the Fe element is also doped in it, but its content is less than 5%. The C atom content of SFC is higher than that of Fe<sub>3</sub>-SFC, while N and O are lower than Fe<sub>3</sub>-SFC. C1s can be deconvoluted into distinct peaks, as seen in Figure 5c. Three distinctive peaks in SFC and Fe<sub>3</sub>-SFC are attributed to C-C/C=C, C-H, and C-OH bonds, respectively, at energies of 284.8, 285.5, and 286.4 eV [53]. The N1s spectra of the two materials can be deconvoluted into three peaks (Figure 5d). These characteristic peaks at 401.09, 399.8, and 398.4 eV can be attributed to graphitic N, pyrrolic N, and pyridine N, respectively [57], and the major peaks for both are graphitic N. Figure 5e shows the XPS spectra of O1s for the two materials. The O1s XPS spectrum of SFC is divided into three peaks: C-OH (531.6 eV), O-H (533.7 eV), and C=O (532.7 eV). Fe<sub>3</sub>-SFC has one more peak than SFC at 530.4 eV, which is Fe-O [58]. In addition, Figure 5f shows the Fe 2p spectrum, in which the two peaks at roughly 713.7 and 725.5 eV, correspond to Fe<sup>3+</sup> 2p<sub>3/2</sub> and Fe<sup>3+</sup> 2p<sub>1/2</sub> in Fe<sub>3</sub>-SFC [55]. The peak at 711.6 eV belongs to the 2p<sub>1/2</sub> peak of Fe<sup>2+</sup> [59]. The two peaks at 723.2 and 718.5 eV can be ascribed to Fe<sup>2+</sup> and Fe 2p<sub>3/2</sub>, respectively, indicating the presence of Fe<sup>0</sup> species on the Fe<sub>3</sub>-SFC surface [58].

### 3.2. TC Degradation

The TC adsorption and catalytic properties of SFC and Fe<sub>n</sub>-SFC were investigated. When comparing Figure 6a,b, it can be shown that after adding PDS, both SFC and Fe<sub>n</sub>-SFC have a greater removal effect. In the instance of PDS, the TC degradation was investigated. After 60 min, the degradation effect of SFC on TC was very limited, at only 19.2%. However, in the Fe<sub>n</sub>-SFC/PDS system, except Fe<sub>4</sub>-SFC, the TC degradation rate of the other modified catalysts could reach more than 75.0% (Figure 6b). The findings demonstrate that adding FeCl<sub>3</sub> considerably improved the capacity to remove TC. In a certain range, the removal rate increased as the FeCl<sub>3</sub> level increased. When FeCl<sub>3</sub>:SFC = 3:1, the highest degradation efficiency can reach 91.5%. When FeCl<sub>3</sub>:SFC = 4:1, the degradation of catalytic performance is even less than that of blank biochar. This indicates that the amount of FeCl<sub>3</sub> has reached saturation, and when FeCl<sub>3</sub>:SFC = 3:1, excessive FeCl<sub>3</sub> may take up reaction sites on the

biochar surface and reduce the degradation efficiency. It proved that  $\text{FeCl}_3\text{:SFC} = 3\text{:}1$  is the best ratio to remove TC.

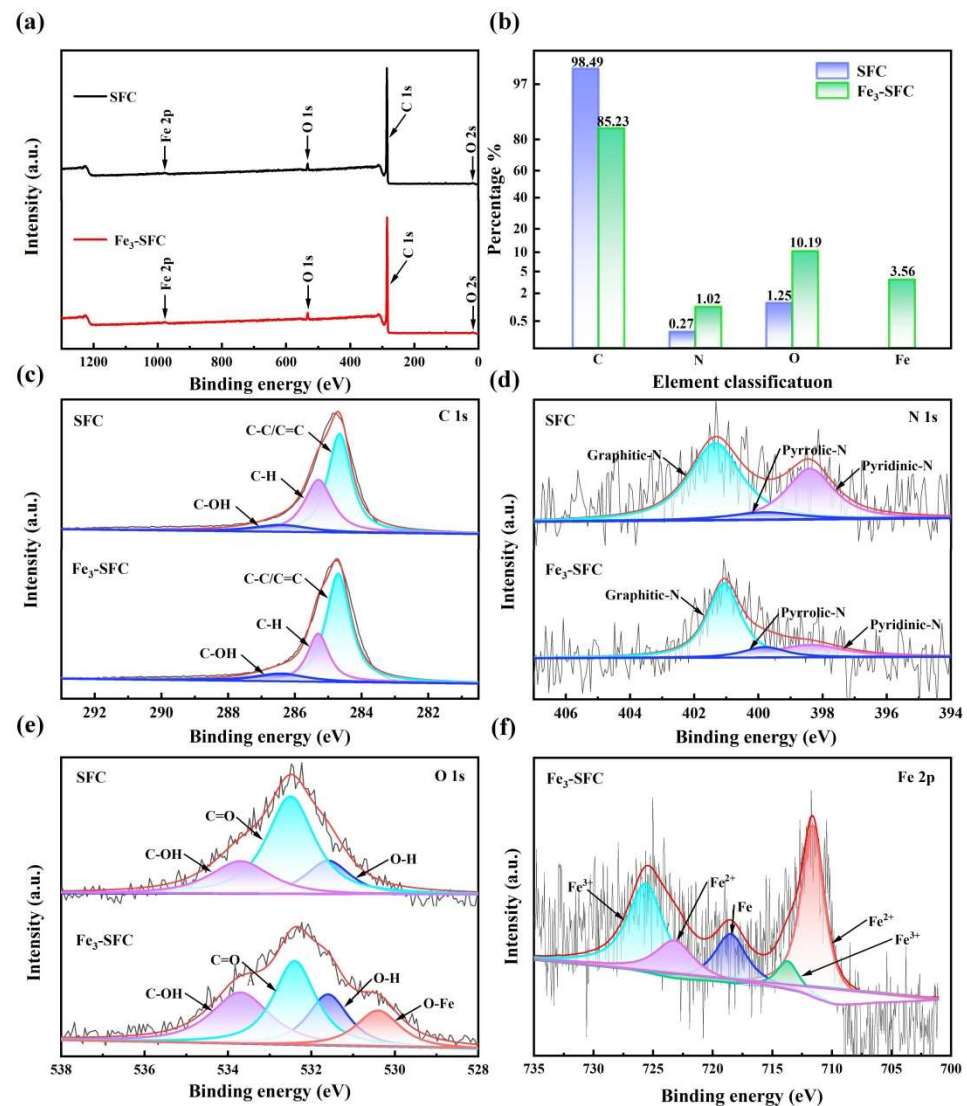


**Figure 5.** XPS survey scan of SFC and  $\text{Fe}_3\text{-SFC}$  (a); proportion of C, N, O, and Fe content (b); C1s peaks of SFC and  $\text{Fe}_3\text{-SFC}$  (c); N1s peaks of SFC and  $\text{Fe}_3\text{-SFC}$  (d); O1s peaks of SFC and  $\text{Fe}_3\text{-SFC}$  (e); Fe2p peaks of SFC and  $\text{Fe}_3\text{-SFC}$  (f).

Characterization of TC degradation in  $\text{Fe}_3\text{-SFC/PDS}$  systems using pseudo-first-order and pseudo-second-order kinetics (Equations (1) and (2)) [60,61].

$$\ln(C_0/C_t) = k_1 t \quad (3)$$

$$1/C_t - 1/C_0 = k_2 t \quad (4)$$

TC concentrations at time 0 and  $t$  are represented by  $C_0$  and  $C_t$ . The first- and second-order rate constants are denoted by  $k_1$  and  $k_2$ , respectively. Equations (1) and (2) were used to monitor the TC-degrading kinetic model in the  $\text{Fe}_3\text{-SFC/PDS}$  system (Figure 6c,d). The second-order model fitting's correlation coefficient ( $R^2$ ) is 0.998, greater than the first-order model's (0.924) (Table 2). This outcome proves that the second-order reaction kinetics are better suited for TC degradation in the  $\text{Fe}_3\text{-SFC/PDS}$  system [61].

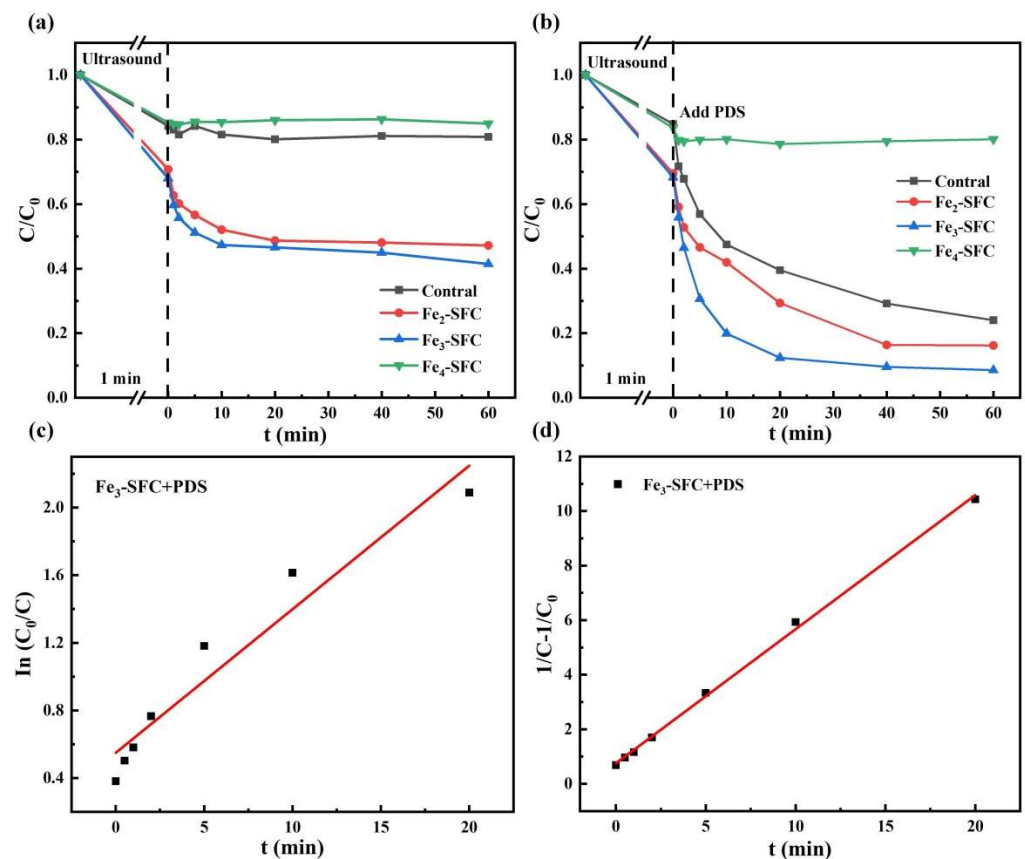


**Figure 6.** TC adsorption by the different biochar (a); TC degradation by the different biochar (b) the pseudo-first-order kinetic fitting curve (c); and the pseudo-second-order kinetics fitting curve (d).

**Table 2.** Fitting results regarding the degradation of TC in Fe<sub>3</sub>-SFC/PDS system.

Fitting Formula	Dynamical Equation	k	R <sup>2</sup>
Pseudo-first-order kinetic	$-\ln(C_0/C_t) = 0.085t + 0.549$	$0.085 \text{ min}^{-1}$	0.924
Pseudo-second-order kinetic	$1/C_t - 1/C_0 = 0.491t + 0.756$	$0.491 \cdot \text{L} \cdot \text{mg}^{-1} \cdot \text{min}^{-1}$	0.998

Figure 7a shows that Fe<sub>3</sub>-SFC dosage had a favorable effect on TC degradation, as degradation rate of TC also increased from 81.9% to 92.3% as the amount of Fe<sub>3</sub>-SFC was enhanced from 0.05 g/L to 0.15 g/L. This suggested that high doses of Fe<sub>3</sub>-SFC could effectively improve the removal rate of TC, as more Fe<sub>3</sub>-SFC could certify more active sites for activating PDS, thereby increasing the activation efficiency [62]. Figure 7b depicts the result of PDS concentration on degradation of TC. With an increase in PDS concentration, it was seen that the rate of TC degradation decreased, probably because excessive PDS would react with active oxidizing species to form some substances with low oxidation performance. But the amount of PDS had little impact on the catalytic degradation performance of the Fe<sub>3</sub>-SFC/PDS system [63]. Figure 7c shows that, as the initial concentration of TC increases, its degradation rate decreased, which indicated that active sites on the Fe<sub>3</sub>-SFC surface are more easily occupied by TC. Therefore, the contact between PDS and Fe<sub>3</sub>-SFC is reduced [64].

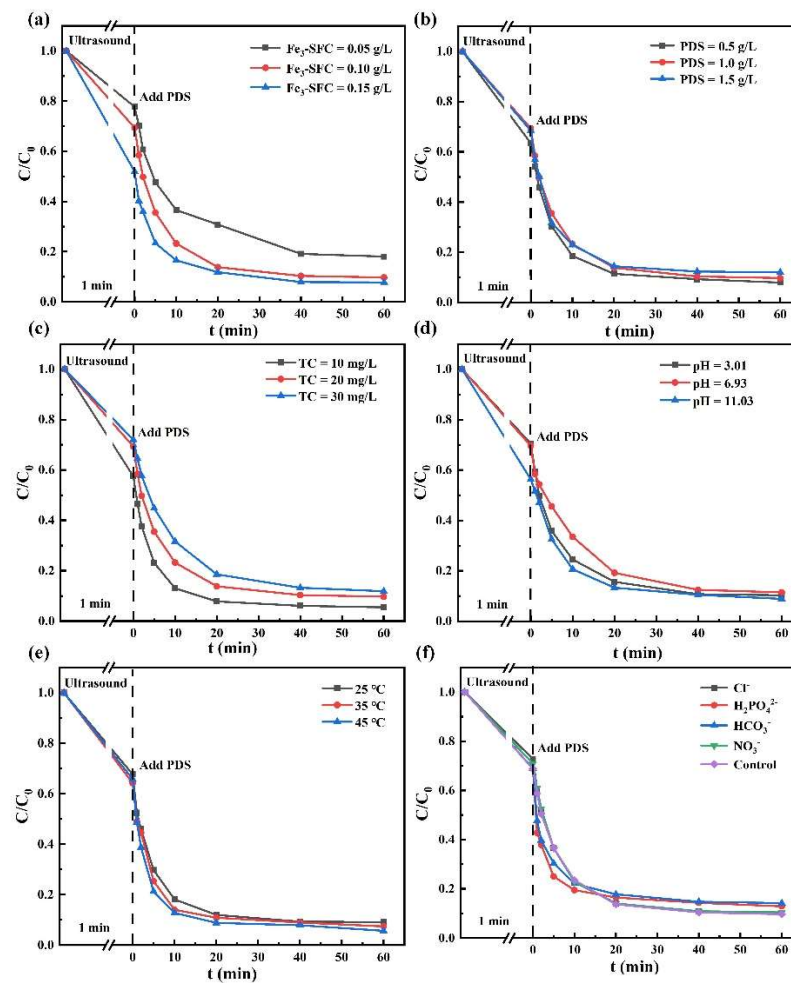
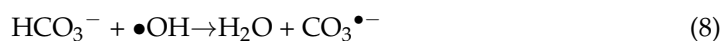


**Figure 7.** The influence of catalyst dosage (a); PDS dosage (b); TC concentrations (c); initial pH (d); temperature of reaction (e) and anions (f) on the degradation of TC in the  $\text{Fe}_3\text{-SFC/PDS}$  system.

Within the  $\text{Fe}_3\text{-SFC/PDS}$  system, the effect of initial pH ranging from 3.01 to 11.03 on TC degradation is shown in Figure 7d. Over a pH range of 3.01 to 11.03, nearly overlapping TC degradation curves were obtained, indicating that  $\text{Fe}_3\text{-SFC}$  was catalytically stable over a wide working pH range [65,66]. When temperature increased from 25 °C to 35 °C, TC degradation rate increased slightly, but was almost unchanged (Figure 7e), which showed that higher temperature could enhance the catalytic performance of the  $\text{Fe}_3\text{-SFC/PDS}$  system, which was due to the higher temperature. High temperature could activate PDS to produce more active species, but the effect of this change was relatively weak [61]. Figure 7f shows the effects of  $\text{Cl}^-$ ,  $\text{H}_2\text{PO}_4^{2-}$ ,  $\text{HCO}_3^-$ , and  $\text{NO}_3^-$  on the degradation efficiency of TC. The existence of four anions showed different degrees of inhibition on the degradation of TC.  $\text{Cl}^-$  and  $\text{NO}_3^-$  had only a minor inhibitory effect.  $\text{Cl}^-$  can react with  $\text{SO}_4^{\bullet-}$  to form  $\text{Cl}^\bullet$  with relatively weak oxidizing power [67], and  $\text{NO}_3^-$  possessed a quenching effect on  $\bullet\text{OH}$  [61]. Relatively strong inhibition of TC degradation by  $\text{HPO}_4^{2-}$  and  $\text{HCO}_3^-$ .  $\text{HCO}_3^-$  had a powerful removal effect on  $\text{SO}_4^{\bullet-}$  and  $\bullet\text{OH}$ , thus decreasing TC degradation efficiency [68].  $\text{HPO}_4^{2-}$  in-solution was also the scavenger of  $\bullet\text{OH}$  and  $\text{SO}_4^{\bullet-}$  [69]. In addition,  $\text{HPO}_4^{2-}$  could form complexes with surface metal ions on  $\text{Fe}_3\text{-SFC/PDS}$ , and the active sites on the catalyst surface would be covered by complexes [70], thus hindering the TC degradation.





The reusability of Fe<sub>3</sub>-SFC was investigated (Figure 8). Three recovery experiments were performed on Fe<sub>3</sub>-SFC. After each experiment, recovery, washing and drying of the spent N-BC catalyst were performed. It could be seen that degradation of TC in three runs were 90.5%, 83.9% and 51.4% after 60 min of reaction, respectively. With the increase of recycling times, TC degradation gradually decreases, which might be due to reduction of surface functional groups and coverage of active sites by intermediates, e.g., [66], which indicated that Fe<sub>3</sub>-SFC had a certain lifetime before being consumed in the reaction. However, the degradation rate after three recycling cycles was 51.4%, indicating that Fe<sub>3</sub>-SFC still had the ability to remove TC from the aquatic environment [44].

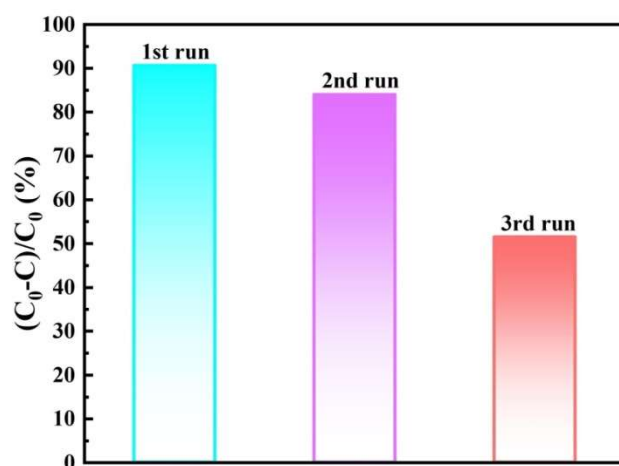


Figure 8. Reusability experiment of Fe<sub>3</sub>-SFC.

Table 3 compares the degradation of pollutants by Fe<sub>3</sub>-SFC and other biochar catalysts.

Table 3. Comparison of Fe<sub>3</sub>-SFC and other materials in terms of pollutant degradation.

Catalysts	Target Pollutants	Catalyst Dosage (G/L)	Pollutant Concentration (Mg/L)	Persulfated dosage (G/L)	Reaction Time	Degradation Conditions	D.E. (%)	Ref.
Fe <sub>3</sub> -SFC	Tetracycline	0.1	10	0.4	1 h	pH: 6.93 T: 25 °C	91.50	This work
KOH activation biochar	Tetracycline	0.2	50	2	3 h	pH: 7 T: 25 °C	82.36	[66]
Goethite/biochar N-doped	Tetracycline	0.5	20	0.1	1 h	pH: 7 T: 25 °C	66.71	[64]
Enteromorpha prolifera-derived magnetic biochar	Tetracycline	0.2	50	0.4	5 h	pH: 4 T: 25 °C	87.2	[71]
Passion fruit shell-derived biochar	Tetracycline	0.4	20	0.1	2 h	pH: 7 T: 25 °C	90.91	[61]
Black fungus-derived N-doped biochar	Tetracycline	0.3	20	0.4	1 h	pH: 6.9 T: 25 °C	89.8	[53]
Fe(II)-rich potassium-doped magnetic biochar	Metronidazole	0.5	20	10 mM	120 min	pH: 6.5 T: 25 °C	98.4	[72]
Fe, N co-doped biochar (Fe-N-BC)	Acid orange	0.2	20	1 mM	40 min	pH: 3 T: 25 °C	100	[57]

Table 3. Cont.

Catalysts	Target Pollutants	Catalyst Dosage (G/L)	Pollutant Concentration (Mg/L)	Persulfate dosage (G/L)	Reaction Time	Degradation Conditions	D.E. (%)	Ref.
Composite of iron sulfide and biochar (FeS@BC)	Tetracycline	0.3	200	10 mM	30 min	pH: 3.6 T: 25 °C	87.4	[73]
Magnetic rape straw biochar (MRSB)	Tetracycline hydrochloride	1	20	8 mM	120 min	pH: 5.68 T: 25 °C	98.02	[74]
Magnetic biochar was prepared from dewatered piggery sludge	Tetracycline	0.75	6.7	20 mg/L	120 min	pH: 7 T: 25 °C	66.87	[75]
Biochar supported nanosized iron (nFe(0)/BC)	Tetracycline	0.4	100	1 mM	240 min	pH: 5 T: 25 °C	97.68	[76]

### 3.3. Reaction Mechanism

To better grasp degradation mechanism of TC and discern active substances in the system, quenching experiments were performed on the Fe<sub>3</sub>-SFC/PDS system. Ethanol (EtOH) had been reported to be a typical •OH and SO<sub>4</sub><sup>•−</sup> trap, and *t*-butanol (TBA) was supposed to be able to capture •OH [77,78]. Singlet oxygen (<sup>1</sup>O<sub>2</sub>) could be largely trapped by furfuryl alcohol (FFA) [79]. Figure 9a shows that TC degradation efficiency was significantly reduced in the presence of FFA, whereas the degradation efficiency of TC decreased only slightly in the presence of TBA or EtOH. This result demonstrated that the Fe<sub>3</sub>-SFC/PDS system produced a large amount of <sup>1</sup>O<sub>2</sub> and a bit of •OH and SO<sub>4</sub><sup>•−</sup>, indicating that main active species for degrading TC was <sup>1</sup>O<sub>2</sub>. In order to further confirm existence of <sup>1</sup>O<sub>2</sub> in this system, it was measured using EPR technique. A strong signal of TEMP <sup>1</sup>O<sub>2</sub> was heeded in the Fe<sub>3</sub>-SFC/PDS-TEMP system, as shown in Figure 9b, indicating the presence of <sup>1</sup>O<sub>2</sub> in the Fe<sub>3</sub>-SFC/PDS-TEMP system [61].

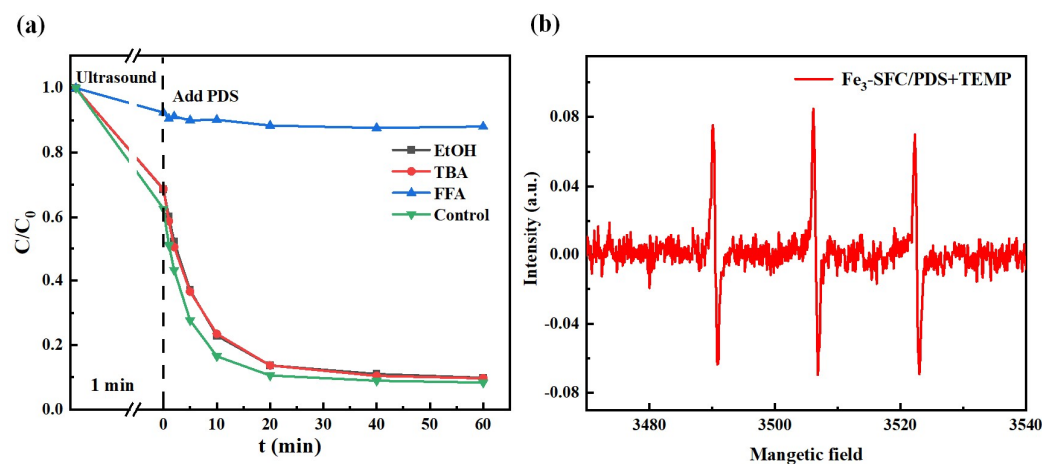
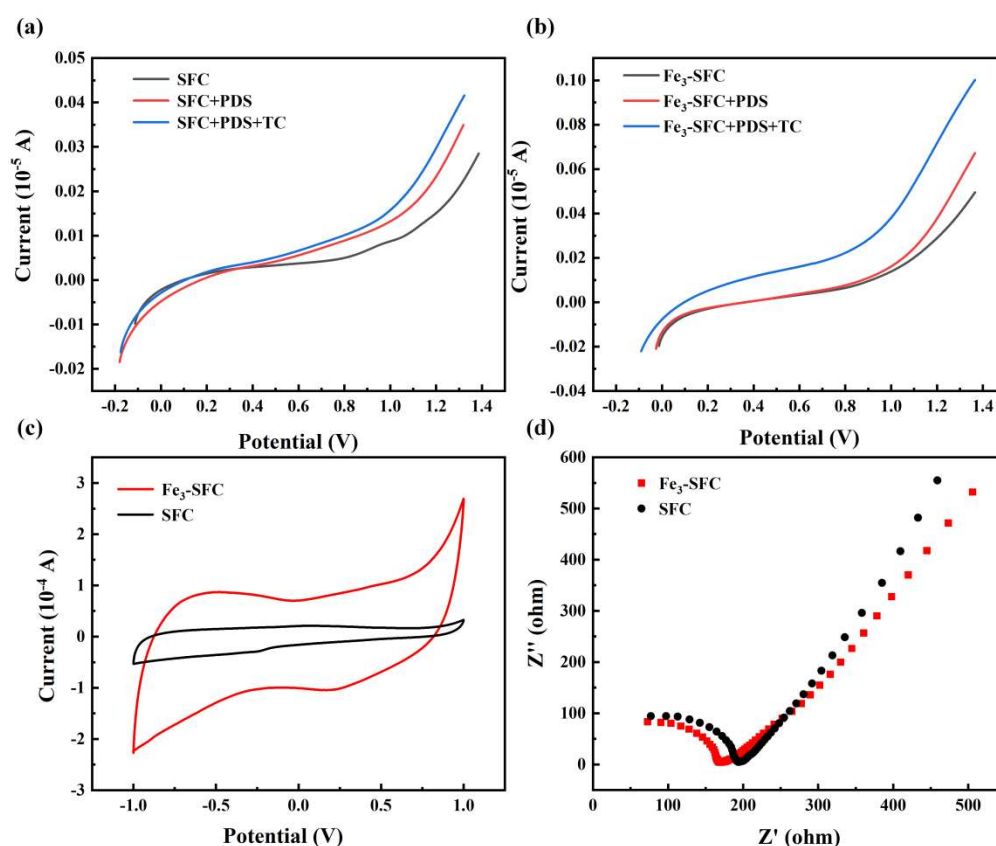


Figure 9. Effects of different quenchers on TC degradation in Fe<sub>3</sub>-SFC/PDS system (a) and the EPR spectrum in Fe<sub>3</sub>-SFC/PDS system with TEMP (b).

Figure 10 shows the LSV curves, CV curves, and EIS analysis of SFC and Fe<sub>3</sub>-SFC under different conditions. The conduction of biochar could be clarified by electrochemical measurement [80]. Through the LSV diagrams of the two materials (Figure 10a,b), it could be found that the current increases significantly [81] with the increase of PDS solution. This indicates the interaction and electron rearrangement between PDS and biochar-based catalysts [82]. It is worth noting that injecting TC afterward caused another current increase, demonstrating that electron transfer [83] was faster in the PDS/SFC or Fe<sub>3</sub>-SFC/TC ternary system. The birth material carbon was thought to act as a bridge for the formed current, promoting electron transfer from the TC molecule to the PDS [84]. When the currents of the

two systems were compared, it could be said that the current of Fe<sub>3</sub>-SFC was significantly higher than that of SFC, indicating that Fe<sub>3</sub>-SFC had a better electron transfer ability than SFC [85].



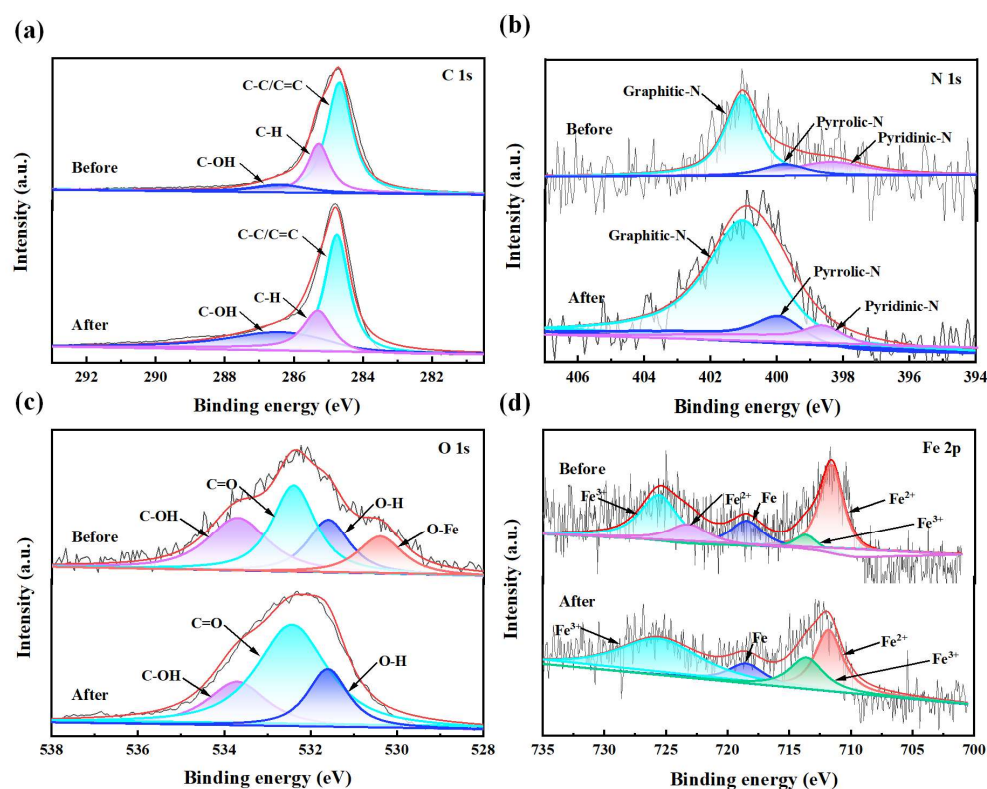
**Figure 10.** LSV curve of SFC (a) and Fe<sub>3</sub>-SFC (b) in different situations; CV curves of SFC and Fe<sub>3</sub>-SFC (c); EIS analysis of SFC and Fe<sub>3</sub>-SFC (d).

From Figure 10c, it is worth noting that closed area of Fe<sub>3</sub>-SFC in the current potential curve is much larger than that of SFC [86], indicating that Fe<sub>3</sub>-SFC has a large charge storage capacity to accept electrons [87]. The results of LSV and CV further confirmed that catalytic performance of Fe<sub>3</sub>-SFC for PDS activation was higher than SFC.

EIS tests were performed to further investigate electron transfer ability of two carbon-based catalysts (Figure 10d). The electron transfer ability of biochar-based catalysts is described according to the diameter of the semicircle [88]. The semicircle diameter of Fe<sub>3</sub>-SFC is significantly smaller than that of SFC. The impedance order of biochar is Fe<sub>3</sub>-SFC < SFC. This is very consistent with their catalytic performance results. It can be concluded that the incorporation of Fe may improve the electron density and promote the electron flow. In the original structure, doping Fe atoms will help with electron triggering and transfer [89].

In order to facilitate electron transfer between the catalyst and the PDS molecule and facilitate the degradation of organic pollutants, catalytic activation aims to weaken and break down the superoxide O-O link in PDS [61]. XPS spectra of Fe<sub>3</sub>-SFC before and after the reaction reveal the activation mechanism of PDS (Figure 11). Figure 11a shows that the content of C-C/C=C functional groups in Fe<sub>3</sub>-SFC decreased from 65.3% to 50.4% after the reaction, which indicated that C-C/C=C was the main reactive functional group to activate PDS [74]. The content of pyridinic N decreased by 18.75% after the reaction, as shown in Figure 11b, indicating that pyridinic N was involved in the activation of PDS [58]. Although graphite N did not change much, previous studies had proved that graphite N could accelerate the transfer of electrons between adjacent ones and destroy the inertia of networks of C, thereby increasing the positive charge of C [61], which was beneficial to pass. PDS was activated by a positively charged nucleophilic reaction that produces

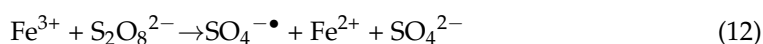
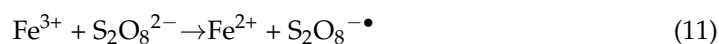
$^1\text{O}_2$ , implying that graphite N was involved in the process. After the reaction, the O-Fe in Fe<sub>3</sub>-SFC vanished (Figure 11c), which indicated that O-Fe was the main reactive site when Fe<sub>3</sub>-SFC catalyzed PDS degradation of TC [74]. After the reaction, the Fe<sup>2+</sup> bond in the XPS of Fe<sub>3</sub>-SFC (Figure 11d) disappeared and the Fe<sup>2+</sup> 2p<sub>1/2</sub> bond area decreased, demonstrating that Fe<sup>2+</sup> served as a PDS-activating functional group and was involved in the degradation of TC, which further confirmed that Fe<sub>3</sub>-SFC was involved in the reaction of ferrous iron [76]. The reason why Fe<sup>2+</sup> 2p<sub>1/2</sub> still exists at this time is that high-energy Fe<sup>2+</sup> is more likely to react [90].



**Figure 11.** XPS spectra of C1s (a); O1s (b); N1s (c) and Fe2p (d) of Fe<sub>3</sub>-SFC before and after reaction.

Based on the above analysis, the radical ( $\text{SO}_4^{\bullet-}$  and  $\bullet\text{OH}$ ) and non-radical ( $^1\text{O}_2$  and electron transfer) pathways were used to degrade TC in the Fe<sub>3</sub>-SFC/PDS system, with the latter playing a dominant role (Figure 9a). O-Fe in Fe<sub>3</sub>-SFC disappeared after the reaction, according to the O1s-XPS spectra of Fe<sub>3</sub>-SFC before and after the reaction, showing that O-Fe was the primary reaction site [91]. Relevant studies had shown that the content of active ingredients in magnetic BC, especially Fe (II), was closely related to its activation properties. The Fe<sup>2+</sup> bond in the XPS of Fe<sub>3</sub>-SFC vanished after the reaction, demonstrating that Fe<sup>2+</sup> may have acted as a PDS-activating functional group to encourage  $^1\text{O}_2$  production and was implicated in the degradation of TC. Furthermore,  $^1\text{O}_2$  was produced by the nucleophilic reaction between the three positively charged C ions surrounding graphite N and PDS. In addition to active species, TC degradation may result from the electron transfer (Figure 10b). Rapid TC degradation might be caused by  $^1\text{O}_2$  and electron transfer in the Fe<sub>3</sub>-SFC/PDS oxidation system, whereas  $\bullet\text{OH}$  and  $\text{SO}_4^{\bullet-}$  played an adjuvant function in TC degradation.

The reversible transformation of Fe<sup>2+</sup> and Fe<sup>3+</sup> is shown in Figure 12, and the main reactions involved are [92]:



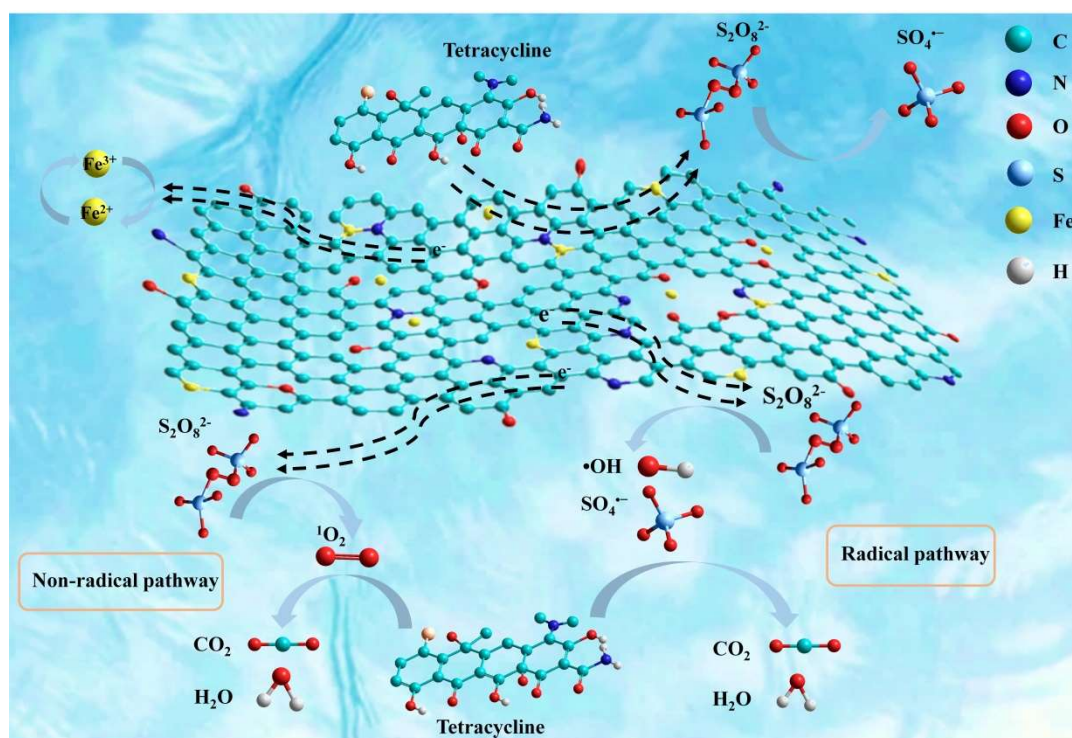


**Figure 12.** Mechanism of the degradation of TC in  $\text{Fe}_3\text{-SFC/PDS}$  system.

In the experiments of Xie et al. [93], the Fe concentration in wastewater discharge after Fe-doped catalyst was degraded by TC was lower than the standard limits from environmental requirements for China's surface water (GB 3838-2002). In this paper, Fe-modified catalysts containing less Fe are used, and the Fe content of the degraded water is low. This will not pollute the environment in a secondary way.

#### 4. Conclusions

In this research, using ferric chloride and sterculia foetida as raw materials, a novel magnetic biochar ( $\text{Fe}_3\text{-SFC}$ ) was successfully synthesized as a persulfate activator to efficiently degrade TC. The characterization results showed that the  $\text{Fe}_3\text{-SFC}$  surface was significantly coated with iron corrosion products but less content, and the surface's low-valent Fe (II) on the surface participated in the activation of PDS and was converted into high-valent Fe (III). When the dose of  $\text{Fe}_3\text{-SFC}$  is increased, the efficiency of TC's degradation increases, and high TC concentrations will have low degradation efficiencies. PDS concentration (0.5 to 1.5 g/L), solution pH (3.01 to 11.03) and reaction temperature (25 to 45 °C) have little influence on TC degradation. In the presence of  $\text{HPO}_4^{2-}$  and  $\text{HCO}_3^-$ , the TC degradation in the  $\text{Fe}_3\text{-SFC/PDS}$  system was restrained. The degradation mechanism of TC in the  $\text{Fe}_3\text{-SFC/PDS}$  system revealed that non-radical pathways involving  $^1\text{O}_2$ , electron transfer, and Fe (II) played a significant role. At the same time, there are some phenomena such as low preparation yield, poor magnetic properties and low recovery rate of  $\text{Fe}_3\text{-SFC}$  observed in this experiment. Therefore, the  $\text{Fe}_3\text{-SFC}$  synthesized in this study has important practical significance in PS-activated degradation of TC.

**Author Contributions:** Conceptualization, Y.Z., X.J., Z.K. and Z.H.; writing—original draft preparation, Y.Z.; writing—review and editing, Y.Z., X.J., Z.K. and X.K.; visualization, X.K., M.G. and Z.H.; supervision, C.W., J.W. and Z.H.; project administration, C.W., D.Z. and Z.H.; funding acquisition, Z.H. All authors have read and agreed to the published version of the manuscript.

**Funding:** This work was supported by the Hebei National Science Fund for Distinguished Young Scholars (No. E2019209433), Youth Talent Program of Department of Education of Hebei Province (No. BJ2018020) and Hebei Province High-level Talents Funded Project (No. B2020003030).

**Institutional Review Board Statement:** Not applicable.

**Informed Consent Statement:** Not applicable.

**Data Availability Statement:** No data reported.

**Conflicts of Interest:** The authors declare no conflict of interest.

## References

1. Yue, Y.; Shen, C.; Ge, Y. Biochar accelerates the removal of tetracyclines and their intermediates by altering soil properties. *J. Hazard. Mater.* **2019**, *380*, 120821. [[CrossRef](#)] [[PubMed](#)]
2. Wang, T.; Mei, Q.; Tao, Z.; Wu, H.; Zhao, M.; Wang, S.; Liu, Y. A smartphone-integrated ratiometric fluorescence sensing platform for visual and quantitative point-of-care testing of tetracycline. *Biosens. Bioelectron.* **2020**, *148*, 111791. [[CrossRef](#)] [[PubMed](#)]
3. Kang, Z.; Jia, X.; Zhang, Y.; Kang, X.; Ge, M.; Liu, D.; Wang, C.; He, Z. A Review on Application of Biochar in the Removal of Pharmaceutical Pollutants through Adsorption and Persulfate-Based AOPs. *Sustainability* **2022**, *14*, 10128. [[CrossRef](#)]
4. Ao, X.; Sun, W.; Li, S.; Yang, C.; Li, C.; Lu, Z. Degradation of tetracycline by medium pressure UV-activated peroxymonosulfate process: Influencing factors, degradation pathways, and toxicity evaluation. *Chem. Eng. J.* **2019**, *361*, 1053–1062. [[CrossRef](#)]
5. Hayati, B.; Mahmoodi, N.M. Modification of activated carbon by the alkaline treatment to remove the dyes from wastewater: Mechanism, isotherm and kinetic. *Desalination Water Treat.* **2012**, *47*, 322–333. [[CrossRef](#)]
6. Xie, Z.; Feng, Y.; Wang, F.; Chen, D.; Zhang, Q.; Zeng, Y.; Lv, W.; Liu, G. Construction of carbon dots modified MoO<sub>3</sub>/g-C<sub>3</sub>N<sub>4</sub> Z-scheme photocatalyst with enhanced visible-light photocatalytic activity for the degradation of tetracycline. *Appl. Catal. B Environ.* **2018**, *229*, 96–104. [[CrossRef](#)]
7. Song, Y.; Qi, J.; Tian, J.; Gao, S.; Cui, F. Construction of Ag/g-C<sub>3</sub>N<sub>4</sub> photocatalysts with visible-light photocatalytic activity for sulfamethoxazole degradation. *Chem. Eng. J.* **2018**, *341*, 547–555. [[CrossRef](#)]
8. Mahmoodi, N.M.; Hayati, B.; Arami, M. Textile dye removal from single and ternary systems using date stones: Kinetic, isotherm, and thermodynamic studies. *J. Chem. Eng. Data* **2010**, *55*, 4638–4649. [[CrossRef](#)]
9. Goswami, R.K.; Agrawal, K.; Verma, P. Multifaceted Role of Microalgae for Municipal Wastewater Treatment: A Futuristic Outlook toward Wastewater Management. *Clean Soil Air Water* **2021**. [[CrossRef](#)]
10. Ahmed, M.; Nasar, A. Utilization of Jackfruit Peel as a Low-cost Adsorbent for the Removal of Methylene Blue Dye from Synthetically Polluted Water. *Curr. Anal. Chem.* **2021**, *17*, 1016–1026. [[CrossRef](#)]
11. Gao, Y.; Wang, Q.; Ji, G.; Li, A. Degradation of antibiotic pollutants by persulfate activated with various carbon materials. *Chem. Eng. J.* **2022**, *429*, 132387. [[CrossRef](#)]
12. Gao, J.; Han, D.; Xu, Y.; Liu, Y.; Shang, J. Persulfate activation by sulfide-modified nanoscale iron supported by biochar (S-nZVI/BC) for degradation of ciprofloxacin. *Sep. Purif. Technol.* **2020**, *235*, 116202. [[CrossRef](#)]
13. Li, R.; Lu, X.; Yan, B.; Li, N.; Chen, G.; Cheng, Z.; Hou, L.A.; Wang, S.; Duan, X. Sludge-derived biochar toward sustainable Peroxymonosulfate Activation: Regulation of active sites and synergistic production of reaction oxygen species. *Chem. Eng. J.* **2022**, *440*, 135897. [[CrossRef](#)]
14. Huang, R.; Yang, J.; Cao, Y.; Dionysiou, D.D.; Wang, C. Peroxymonosulfate catalytic degradation of persistent organic pollutants by engineered catalyst of self-doped iron/carbon nanocomposite derived from waste toner powder. *Sep. Purif. Technol.* **2022**, *291*, 120963. [[CrossRef](#)]
15. Wang, C.; Huang, R.; Sun, R.; Yang, J.; Sillanpää, M. A review on persulfates activation by functional biochar for organic contaminants removal: Synthesis, characterizations, radical determination, and mechanism. *J. Environ. Chem. Eng.* **2021**, *9*, 106267. [[CrossRef](#)]
16. Zhong, M.-e.; Guan, J.; Feng, Q.; Wu, X.; Xiao, Z.; Zhang, W.; Tong, S.; Zhou, N.; Gong, D. Accelerated polysulfide redox kinetics revealed by ternary sandwich-type S@Co/N-doped carbon nanosheet for high-performance lithium-sulfur batteries. *Carbon* **2018**, *128*, 86–96. [[CrossRef](#)]
17. Mahmoodi, N.M. Photocatalytic degradation of dyes using carbon nanotube and titania nanoparticle. *Water Air Soil Pollut.* **2013**, *224*, 1–8. [[CrossRef](#)]
18. Oveisi, M.; Asli, M.A.; Mahmoodi, N.M. Carbon nanotube based metal-organic framework nanocomposites: Synthesis and their photocatalytic activity for decolorization of colored wastewater. *Inorg. Chim. Acta* **2019**, *487*, 169–176. [[CrossRef](#)]
19. Ren, T.-L.; Ma, X.-W.; Wu, X.-Q.; Yuan, L.; Lai, Y.-L.; Tong, Z.-H. Degradation of imidazolium ionic liquids in a thermally activated persulfate system. *Chem. Eng. J.* **2021**, *412*, 128624. [[CrossRef](#)]
20. Gao, Y.-Q.; Gao, N.-Y.; Chu, W.-H.; Zhang, Y.-F.; Zhang, J.; Yin, D.-Q. UV-activated persulfate oxidation of sulfamethoxypyridazine: Kinetics, degradation pathways and impact on DBP formation during subsequent chlorination. *Chem. Eng. J.* **2019**, *370*, 706–715. [[CrossRef](#)]
21. Mahmoodi, N.M.; Saffar-Dastgerdi, M.H. Clean Laccase immobilized nanobiocatalysts (graphene oxide-zeolite nanocomposites): From production to detailed biocatalytic degradation of organic pollutant. *Appl. Catal. B Environ.* **2020**, *268*, 118443. [[CrossRef](#)]
22. Wu, L.; Wu, T.; Liu, Z.; Tang, W.; Xiao, S.; Shao, B.; Liang, Q.; He, Q.; Pan, Y.; Zhao, C.; et al. Carbon nanotube-based materials for persulfate activation to degrade organic contaminants: Properties, mechanisms and modification insights. *J. Hazard. Mater.* **2022**, *431*, 128536. [[CrossRef](#)] [[PubMed](#)]

23. Liang, J.; Xu, X.; Qamar Zaman, W.; Hu, X.; Zhao, L.; Qiu, H.; Cao, X. Different mechanisms between biochar and activated carbon for the persulfate catalytic degradation of sulfamethoxazole: Roles of radicals in solution or solid phase. *Chem. Eng. J.* **2019**, *375*, 121908. [[CrossRef](#)]
24. Zhao, Y.; Dai, H.; Ji, J.; Yuan, X.; Li, X.; Jiang, L.; Wang, H. Resource utilization of luffa sponge to produce biochar for effective degradation of organic contaminants through persulfate activation. *Sep. Purif. Technol.* **2022**, *288*, 120650. [[CrossRef](#)]
25. Yin, F.; Wang, C.; Lin, K.-Y.A.; Tong, S. Persulfate activation for efficient degradation of norfloxacin by a rGO-Fe<sub>3</sub>O<sub>4</sub> composite. *J. Taiwan Inst. Chem. Eng.* **2019**, *102*, 163–169. [[CrossRef](#)]
26. Décima, M.A.; Marzeddu, S.; Barchiesi, M.; Di Marcantonio, C.; Chiavola, A.; Boni, M.R. A Review on the Removal of Carbamazepine from Aqueous Solution by Using Activated Carbon and Biochar. *Sustainability* **2021**, *13*, 11760. [[CrossRef](#)]
27. Mahmoodi, N.M.; Moghimi, F.; Arami, M.; Mazaheri, F. Silk degumming using microwave irradiation as an environmentally friendly surface modification method. *Fibers Polym.* **2010**, *11*, 234–240. [[CrossRef](#)]
28. Mahmoodi, N.M.; Najafi, F.; Neshat, A. Poly (amidoamine-co-acrylic acid) copolymer: Synthesis, characterization and dye removal ability. *Ind. Crops Prod.* **2013**, *42*, 119–125. [[CrossRef](#)]
29. Magioglou, E.; Frontistis, Z.; Vakros, J.; Manariotis, I.; Mantzavinos, D. Activation of Persulfate by Biochars from Valorized Olive Stones for the Degradation of Sulfamethoxazole. *Catalysts* **2019**, *9*, 419. [[CrossRef](#)]
30. Salehi, S.; Abdollahi, K.; Panahi, R.; Rahmanian, N.; Shakeri, M.; Mokhtarani, B. Applications of Biocatalysts for Sustainable Oxidation of Phenolic Pollutants: A Review. *Sustainability* **2021**, *13*, 8620. [[CrossRef](#)]
31. Ho, S.H.; Chen, Y.D.; Li, R.; Zhang, C.; Ge, Y.; Cao, G.; Ma, M.; Duan, X.; Wang, S.; Ren, N.Q. N-doped graphitic biochars from C-phycocyanin extracted Spirulina residue for catalytic persulfate activation toward nonradical disinfection and organic oxidation. *Water Res.* **2019**, *159*, 77–86. [[CrossRef](#)] [[PubMed](#)]
32. Chen, C.; Ma, T.; Shang, Y.; Gao, B.; Jin, B.; Dan, H.; Li, Q.; Yue, Q.; Li, Y.; Wang, Y.; et al. In-situ pyrolysis of Enteromorpha as carbocatalyst for catalytic removal of organic contaminants: Considering the intrinsic N/Fe in Enteromorpha and non-radical reaction. *Appl. Catal. B Environ.* **2019**, *250*, 382–395. [[CrossRef](#)]
33. Shen, Y.; Wang, X.; Hu, H.; Jiang, M.; Bai, Y.; Yang, X.; Shu, H. Sheet-like structure FeF<sub>3</sub>/graphene composite as novel cathode material for Na ion batteries. *RSC Adv.* **2015**, *5*, 38277–38282. [[CrossRef](#)]
34. Mohajershojaei, K.; Mahmoodi, N.M.; Khosravi, A. Immobilization of laccase enzyme onto titania nanoparticle and decolorization of dyes from single and binary systems. *Biotechnol. Bioprocess Eng.* **2015**, *20*, 109–116. [[CrossRef](#)]
35. Li, J.; Liu, G.; Liu, B.; Min, Z.; Qian, D.; Jiang, J.; Li, J. Fe-doped CoSe<sub>2</sub> nanoparticles encapsulated in N-doped bamboo-like carbon nanotubes as an efficient electrocatalyst for oxygen evolution reaction. *Electrochim. Acta* **2018**, *265*, 577–585. [[CrossRef](#)]
36. Mashkoo, F.; Nasar, A. Environmental application of agro-waste derived materials for the treatment of dye-polluted water: A Review. *Curr. Anal. Chem.* **2021**, *17*, 904–916. [[CrossRef](#)]
37. Siddeeg, S.M.; Tahoon, M.A.; Alsaiani, N.S.; Shabbir, M.; Rebah, F.B. Application of functionalized nanomaterials as effective adsorbents for the removal of heavy metals from wastewater: A review. *Curr. Anal. Chem.* **2021**, *17*, 4–22. [[CrossRef](#)]
38. Sun, Y.; He, Z.; Wei, Y.; Liu, G.; Liu, R.; Hu, J.; Liu, H.; Zhang, X.; Yuan, G. Wood-Derived Monolithic Carbon Materials and Their Functional Applications. *Clean Soil Air Water* **2022**, *50*, 2100420. [[CrossRef](#)]
39. Fathy, N.A.; El-Khouly, S.M.; El-Shafey, O.I. Modified carbon nanostructures obtained from sugarcane bagasse hydrochar for treating chromium-polluted water. *Curr. Anal. Chem.* **2021**, *17*, 975–988. [[CrossRef](#)]
40. Mahmoodi, N.M.; Taghizadeh, A.; Taghizadeh, M.; Baglou, M.A.S. Surface modified montmorillonite with cationic surfactants: Preparation, characterization, and dye adsorption from aqueous solution. *J. Environ. Chem. Eng.* **2019**, *7*, 103243. [[CrossRef](#)]
41. Mahmoodi, N.M. Synthesis of magnetic carbon nanotube and photocatalytic dye degradation ability. *Environ. Monit. Assess.* **2014**, *186*, 5595–5604. [[CrossRef](#)] [[PubMed](#)]
42. Jin, Z.; Wang, B.; Ma, L.; Fu, P.; Xie, L.; Jiang, X.; Jiang, W. Air pre-oxidation induced high yield N-doped porous biochar for improving toluene adsorption. *Chem. Eng. J.* **2020**, *385*, 123843. [[CrossRef](#)]
43. Zhang, J.; Wang, Q. Sustainable mechanisms of biochar derived from brewers' spent grain and sewage sludge for ammonia-nitrogen capture. *J. Clean. Prod.* **2016**, *112*, 3927–3934. [[CrossRef](#)]
44. Mei, Y.; Xu, J.; Zhang, Y.; Li, B.; Fan, S.; Xu, H. Effect of Fe-N modification on the properties of biochars and their adsorption behavior on tetracycline removal from aqueous solution. *Bioresour. Technol.* **2021**, *325*, 124732. [[CrossRef](#)]
45. Li, B.; Jing, F.; Hu, Z.; Liu, Y.; Xiao, B.; Guo, D. Simultaneous recovery of nitrogen and phosphorus from biogas slurry by Fe-modified biochar. *J. Saudi Chem. Soc.* **2021**, *25*, 101213. [[CrossRef](#)]
46. Mahmoodi, N.M.; Sadeghi, U.; Maleki, A.; Hayati, B.; Najafi, F. Synthesis of cationic polymeric adsorbent and dye removal isotherm, kinetic and thermodynamic. *J. Ind. Eng. Chem.* **2014**, *20*, 2745–2753. [[CrossRef](#)]
47. Hussain, G.; Haydar, S. Textile Effluent Treatment Using Natural Coagulant *Opuntia stricta* in Comparison with Alum. *Clean Soil Air Water* **2021**, *49*, 2000342. [[CrossRef](#)]
48. Yang, J.; Huang, R.; Wang, L.; Luo, D.; Wang, C. Efficient degradation of toxic mixed dyes through peroxydisulfate activation by copper/iron nanoparticles loaded on 3D carbon: Synthesis, characterizations, and mechanism. *J. Environ. Chem. Eng.* **2022**, *10*, 107606. [[CrossRef](#)]
49. Reza Samarghandi, M.; Tari, K.; Shabanloo, A.; Salari, M.; Zolghadr Nasab, H. Synergistic degradation of acid blue 113 dye in a thermally activated persulfate (TAP)/ZnO-GAC oxidation system: Degradation pathway and application for real textile wastewater. *Sep. Purif. Technol.* **2020**, *247*, 116931. [[CrossRef](#)]

50. Wang, N.; Ma, W.; Ren, Z.; Du, Y.; Xu, P.; Han, X. Prussian blue analogues derived porous nitrogen-doped carbon microspheres as high-performance metal-free peroxymonosulfate activators for non-radical-dominated degradation of organic pollutants. *J. Mater. Chem. A* **2018**, *6*, 884–895. [[CrossRef](#)]
51. Wang, C.; Huang, R.; Sun, R.; Yang, J.; Dionysiou, D.D. Microplastics separation and subsequent carbonization: Synthesis, characterization, and catalytic performance of iron/carbon nanocomposite. *J. Clean. Prod.* **2022**, *330*, 129901. [[CrossRef](#)]
52. Nasrollahi, N.; Aber, S.; Vatanpour, V.; Mahmoodi, N.M. The effect of amine functionalization of CuO and ZnO nanoparticles used as additives on the morphology and the permeation properties of polyethersulfone ultrafiltration nanocomposite membranes. *Compos. Part B Eng.* **2018**, *154*, 388–409. [[CrossRef](#)]
53. Kang, X.; Jia, X.; Kang, Z.; Zhang, Y.; Zhang, D.; Wei, J.; Guo, A.; Ge, M.; He, Z. Activation of peroxydisulfate by black fungus-derived N-doped biochar for tetracycline degradation via non-radical dominated oxidation pathway. *Surf. Interfaces* **2022**, *31*, 102007. [[CrossRef](#)]
54. Mahmoodi, N.M.; Hayati, B.; Bahrami, H.; Arami, M. Dye adsorption and desorption properties of *Mentha pulegium* in single and binary systems. *J. Appl. Polym. Sci.* **2011**, *122*, 1489–1499. [[CrossRef](#)]
55. Zhang, P.; Tan, X.; Liu, S.; Liu, Y.; Zeng, G.; Ye, S.; Yin, Z.; Hu, X.; Liu, N. Catalytic degradation of estrogen by persulfate activated with iron-doped graphitic biochar: Process variables effects and matrix effects. *Chem. Eng. J.* **2019**, *378*, 122141. [[CrossRef](#)]
56. Li, Z.; Liu, D.; Cai, Y.; Wang, Y.; Teng, J. Adsorption pore structure and its fractal characteristics of coals by N<sub>2</sub> adsorption/desorption and FESEM image analyses. *Fuel* **2019**, *257*, 116031. [[CrossRef](#)]
57. Li, X.; Jia, Y.; Zhou, M.; Su, X.; Sun, J. High-efficiency degradation of organic pollutants with Fe, N co-doped biochar catalysts via persulfate activation. *J. Hazard. Mater.* **2020**, *397*, 122764. [[CrossRef](#)]
58. Xi, M.; Cui, K.; Cui, M.; Ding, Y.; Guo, Z.; Chen, Y.; Li, C.; Li, X. Enhanced norfloxacin degradation by iron and nitrogen co-doped biochar: Revealing the radical and nonradical co-dominant mechanism of persulfate activation. *Chem. Eng. J.* **2021**, *420*, 129902. [[CrossRef](#)]
59. Feng, C.; Guo, Y.; Qiao, S.; Xie, Y.; Zhang, L.; Zhang, L.; Wang, W.; Wang, J. 2-Methylimidazole as a nitrogen source assisted synthesis of a nano-rod-shaped Fe/FeN@N-C catalyst with plentiful FeN active sites and enhanced ORR activity. *Appl. Surf. Sci.* **2020**, *533*, 147481. [[CrossRef](#)]
60. Yang, W.; Liu, G.; Chen, Y.; Miao, D.; Wei, Q.; Li, H.; Ma, L.; Zhou, K.; Liu, L.; Yu, Z. Persulfate enhanced electrochemical oxidation of highly toxic cyanide-containing organic wastewater using boron-doped diamond anode. *Chemosphere* **2020**, *252*, 126499. [[CrossRef](#)]
61. Hu, Y.; Chen, D.; Zhang, R.; Ding, Y.; Ren, Z.; Fu, M.; Cao, X.; Zeng, G. Singlet oxygen-dominated activation of peroxymonosulfate by passion fruit shell derived biochar for catalytic degradation of tetracycline through a non-radical oxidation pathway. *J. Hazard. Mater.* **2021**, *419*, 126495. [[CrossRef](#)] [[PubMed](#)]
62. Song, H.; Li, Q.; Ye, Y.; Pan, F.; Zhang, D.; Xia, D. Degradation of cephalexin by persulfate activated with magnetic loofah biochar: Performance and mechanism. *Sep. Purif. Technol.* **2021**, *272*, 118971. [[CrossRef](#)]
63. Yin, R.; Guo, W.; Wang, H.; Du, J.; Wu, Q.; Chang, J.-S.; Ren, N. Singlet oxygen-dominated peroxydisulfate activation by sludge-derived biochar for sulfamethoxazole degradation through a nonradical oxidation pathway: Performance and mechanism. *Chem. Eng. J.* **2019**, *357*, 589–599. [[CrossRef](#)]
64. Guo, Y.; Yan, L.; Li, X.; Yan, T.; Song, W.; Hou, T.; Tong, C.; Mu, J.; Xu, M. Goethite/biochar-activated peroxymonosulfate enhances tetracycline degradation: Inherent roles of radical and non-radical processes. *Sci. Total Environ.* **2021**, *783*, 147102. [[CrossRef](#)]
65. Peng, X.; Wu, J.; Zhao, Z.; Wang, X.; Dai, H.; Wei, Y.; Xu, G.; Hu, F. Activation of peroxymonosulfate by single atom Co-N-C catalysts for high-efficient removal of chloroquine phosphate via non-radical pathways: Electron-transfer mechanism. *Chem. Eng. J.* **2022**, *429*, 132245. [[CrossRef](#)]
66. Li, J.; Liu, Y.; Ren, X.; Dong, W.; Chen, H.; Cai, T.; Zeng, W.; Li, W.; Tang, L. Soybean residue based biochar prepared by ball milling assisted alkali activation to activate peroxydisulfate for the degradation of tetracycline. *J. Colloid Interface Sci.* **2021**, *599*, 631–641. [[CrossRef](#)] [[PubMed](#)]
67. Geng, G.; Gao, Y.; Zhang, Z.; Gao, K.; Zhang, W.; Song, J. Renewable and robust biomass waste-derived Co-doped carbon aerogels for PMS activation: Catalytic mechanisms and phytotoxicity assessment. *Ecotoxicol. Environ. Saf.* **2021**, *220*, 112381. [[CrossRef](#)]
68. Rafiei, N.; Fatehizadeh, A.; Amin, M.M.; Pourzamani, H.R.; Ebrahimi, A.; Taheri, E.; Aminabhavi, T.M. Application of UV/chlorine processes for the DR83:1 degradation from wastewater: Effect of coexisting anions. *J. Environ. Manag.* **2021**, *297*, 113349. [[CrossRef](#)]
69. Li, M.; Huang, F.; Hu, L.; Sun, W.; Li, E.; Xiong, D.; Zhong, H.; He, Z. Efficient activation of peroxymonosulfate by a novel catalyst prepared directly from electrolytic manganese slag for degradation of recalcitrant organic pollutants. *Chem. Eng. J.* **2020**, *401*, 126085. [[CrossRef](#)]
70. Hu, L.; Zhang, G.; Liu, M.; Wang, Q.; Wang, P. Enhanced degradation of Bisphenol A (BPA) by peroxymonosulfate with Co<sub>3</sub>O<sub>4</sub>-Bi<sub>2</sub>O<sub>3</sub> catalyst activation: Effects of pH, inorganic anions, and water matrix. *Chem. Eng. J.* **2018**, *338*, 300–310. [[CrossRef](#)]
71. Xiong, S.; Deng, Y.; Gong, D.; Tang, R.; Zheng, J.; Li, L.; Zhou, Z.; Su, L.; Liao, C.; Yang, L. Magnetically modified in-situ N-doped *Enteromorpha prolifera* derived biochar for peroxydisulfate activation: Electron transfer induced singlet oxygen non-radical pathway. *Chemosphere* **2021**, *284*, 131404. [[CrossRef](#)] [[PubMed](#)]
72. Luo, J.; Yi, Y.; Ying, G.; Fang, Z.; Zhang, Y. Activation of persulfate for highly efficient degradation of metronidazole using Fe(II)-rich potassium doped magnetic biochar. *Sci. Total Environ.* **2022**, *819*, 152089. [[CrossRef](#)] [[PubMed](#)]

73. He, J.; Tang, J.; Zhang, Z.; Wang, L.; Liu, Q.; Liu, X. Magnetic ball-milled FeS@biochar as persulfate activator for degradation of tetracycline. *Chem. Eng. J.* **2021**, *404*, 126997. [[CrossRef](#)]
74. Huang, H.; Guo, T.; Wang, K.; Li, Y.; Zhang, G. Efficient activation of persulfate by a magnetic recyclable rape straw biochar catalyst for the degradation of tetracycline hydrochloride in water. *Sci. Total Environ.* **2021**, *758*, 143957. [[CrossRef](#)]
75. Luo, X.; Shen, M.; Liu, J.; Ma, Y.; Gong, B.; Liu, H.; Huang, Z. Resource utilization of piggery sludge to prepare recyclable magnetic biochar for highly efficient degradation of tetracycline through peroxymonosulfate activation. *J. Clean. Prod.* **2021**, *294*, 126372. [[CrossRef](#)]
76. Shao, F.; Wang, Y.; Mao, Y.; Shao, T.; Shang, J. Degradation of tetracycline in water by biochar supported nanosized iron activated persulfate. *Chemosphere* **2020**, *261*, 127844. [[CrossRef](#)]
77. Kim, J.; Lee, H.; Lee, J.-Y.; Park, K.-H.; Kim, W.; Lee, J.H.; Kang, H.-J.; Hong, S.W.; Park, H.-J.; Lee, S.; et al. Photosensitized Production of Singlet Oxygen via C60 Fullerene Covalently Attached to Functionalized Silica-coated Stainless-Steel Mesh: Remote Bacterial and Viral Inactivation. *Appl. Catal. B Environ.* **2020**, *270*, 118862. [[CrossRef](#)]
78. Fu, H.; Ma, S.; Zhao, P.; Xu, S.; Zhan, S. Activation of peroxymonosulfate by graphitized hierarchical porous biochar and MnFe<sub>2</sub>O<sub>4</sub> magnetic nanoarchitecture for organic pollutants degradation: Structure dependence and mechanism. *Chem. Eng. J.* **2019**, *360*, 157–170. [[CrossRef](#)]
79. Ma, Y.; Gu, Y.; Jiang, D.; Mao, X.; Wang, D. Degradation of 2,4-DCP using persulfate and iron/E-carbon micro-electrolysis coupling system. *J. Hazard. Mater.* **2021**, *413*, 125381. [[CrossRef](#)]
80. Li, B.; Xue, J.; Han, C.; Liu, N.; Ma, K.; Zhang, R.; Wu, X.; Dai, L.; Wang, L.; He, Z. A hafnium oxide-coated dendrite-free zinc anode for rechargeable aqueous zinc-ion batteries. *J. Colloid Interface Sci.* **2021**, *599*, 467–475. [[CrossRef](#)]
81. Tang, F.; He, T.; Zhang, H.; Wu, X.; Li, Y.; Long, F.; Xiang, Y.; Zhu, L.; Wu, J.; Wu, X. The MnO@N-doped carbon composite derived from electrospinning as cathode material for aqueous zinc ion battery. *J. Electroanal. Chem.* **2020**, *873*, 114368. [[CrossRef](#)]
82. Ye, S.; Zeng, G.; Tan, X.; Wu, H.; Liang, J.; Song, B.; Tang, N.; Zhang, P.; Yang, Y.; Chen, Q.; et al. Nitrogen-doped biochar fiber with graphitization from *Boehmeria nivea* for promoted peroxymonosulfate activation and non-radical degradation pathways with enhancing electron transfer. *Appl. Catal. B Environ.* **2020**, *269*, 118850. [[CrossRef](#)]
83. Xie, X.; Liang, S.; Gao, J.; Guo, S.; Guo, J.; Wang, C.; Xu, G.; Wu, X.; Chen, G.; Zhou, J. Manipulating the ion-transfer kinetics and interface stability for high-performance zinc metal anodes. *Energy Environ. Sci.* **2020**, *13*, 503–510. [[CrossRef](#)]
84. Zhu, K.; Bin, Q.; Shen, Y.; Huang, J.; He, D.; Chen, W. In-situ formed N-doped bamboo-like carbon nanotubes encapsulated with Fe nanoparticles supported by biochar as highly efficient catalyst for activation of persulfate (PS) toward degradation of organic pollutants. *Chem. Eng. J.* **2020**, *402*, 126090. [[CrossRef](#)]
85. Meng, W.; Li, C.; Yao, M.; He, Z.; Wu, X.; Jiang, Z.; Dai, L.; Wang, L. Synthesis and electrochemical performance of Li<sub>1+x</sub>Ti<sub>2-x</sub>Fe<sub>x</sub>(PO<sub>4</sub>)<sub>3</sub>/C anode for aqueous lithium ion battery. *Adv. Powder Technol.* **2020**, *31*, 1359–1364. [[CrossRef](#)]
86. Kong, P.; Zhu, L.; Li, F.; Xu, G. Self-Supporting Electrode Composed of SnSe Nanosheets, Thermally Treated Protein, and Reduced Graphene Oxide with Enhanced Pseudocapacitance for Advanced Sodium-Ion Batteries. *ChemElectroChem* **2019**, *6*, 5642–5650. [[CrossRef](#)]
87. Hu, Q.; Tang, M.; He, M.; Jiang, N.; Xu, C.; Lin, D.; Zheng, Q. Core-shell MnO<sub>2</sub>@CoS nanosheets with oxygen vacancies for high-performance supercapattery. *J. Power Sources* **2020**, *446*, 227335. [[CrossRef](#)]
88. Zhu, S.; Huang, X.; Ma, F.; Wang, L.; Duan, X.; Wang, S. Catalytic Removal of Aqueous Contaminants on N-Doped Graphitic Biochars: Inherent Roles of Adsorption and Nonradical Mechanisms. *Environ. Sci. Technol.* **2018**, *52*, 8649–8658. [[CrossRef](#)]
89. Li, J.; Jiang, J.; Xu, Z.; Liu, M.; Tang, S.; Yang, C.; Qian, D. Facile synthesis of Ag@Cu<sub>2</sub>O heterogeneous nanocrystals decorated N-doped reduced graphene oxide with enhanced electrocatalytic activity for ultrasensitive detection of H<sub>2</sub>O<sub>2</sub>. *Sens. Actuators B Chem.* **2018**, *260*, 529–540. [[CrossRef](#)]
90. Deng, H.; Li, R.; Wang, B.; Ma, M.; Zhong, X. An annularly-distributed poly-stable array for broadband vibrational energy. *Sens. Actuators A Phys.* **2021**, *332*, 113106. [[CrossRef](#)]
91. Wang, J.; Liu, G.; Fan, K.; Zhao, D.; Liu, B.; Jiang, J.; Qian, D.; Yang, C.; Li, J. N-doped carbon coated anatase TiO<sub>2</sub> nanoparticles as superior Na-ion battery anodes. *J. Colloid Interface Sci.* **2018**, *517*, 134–143. [[CrossRef](#)]
92. Li, Y.; Yang, Z.; Zhang, H.; Tong, X.; Feng, J.B. Fabrication of sewage sludge-derived magnetic nanocomposites as heterogeneous catalyst for persulfate activation of Orange G degradation. *Colloids Surf. A Physicochem. Eng. Asp.* **2017**, *529*, 856–863. [[CrossRef](#)]
93. Xie, W.; Shi, Y.; Wang, Y.; Zheng, Y.; Liu, H.; Hu, Q.; Wei, S.; Gu, H.; Guo, Z. Electrospun iron/cobalt alloy nanoparticles on carbon nanofibers towards exhaustive electrocatalytic degradation of tetracycline in wastewater. *Chem. Eng. J.* **2021**, *405*, 126585. [[CrossRef](#)]